Volume 24
Number 1

June *2022*
(ISSN 1109-1606)

Journal of

APPLIED ELECTROMAGNETISM

JAE

Trans Black Sea Region Union of Applied Electromagnetism
BSUAE

Institute of Communication and Computer Systems

Athens - GREECE

Volume 24 **June 2022**
Number 1 **(ISSN 1109-1606)**

JOURNAL
OF
APPLIED ELECTROMAGNETISM

Institute of Communication and Computer Systems

Athens - GREECE

Volume 24 **Number 1**

June 2022

TRANS BLACK SEA REGION UNION OF APPLIED ELECTROMAGNETISM (BSUAE)

JOURNAL OF APPLIED ELECTROMAGNETISM

Institute of Communication and Computer Systems

Athens - GREECE

Journal of Applied Electromagnetism

Copyright Form

The undersigned I confirm that I agree the publication of the article

in the Journal of Applied Electromagnetism and the copyright to belong to Trans Black Sea Union of Applied Electromagnetism. I understand that I have the full right to reuse this manuscript for my own purposes.

Name:

Surname:

Address:

E-mail:

Signed:

***Please send the previous form signed either by e-mail to pfrangos@central.ntua.gr , or by fax to the fax number: +30 210 772 2281, attention of Prof. P. Frangos.**

Address

Institute of Communication and Computer Systems,

National Technical University of Athens,

9, Iroon Polytechniou Str.,

157 73 Athens - GREECE

Tel: (+30) 210 772 3694

Fax: (+30) 210 772 2281, attention of Prof. P. Frangos

e-mail: pfrangos@central.ntua.gr

Web site: **http://jae.ece.ntua.gr**

TRANS BLACK SEA REGION UNION OF APPLIED ELECTROMAGNETISM (BSUAE)

JOURNAL OF APPLIED ELECTROMAGNETISM (JAE)

Volume 24 Number 1 June 2022

CONTENTS

In the present study, a new methodology for solving an eigenvalue problem and the two-dimensional E-polarized electromagnetic wave diffraction by the arbitrary shaped perfect electric conducting (PEC) scatterers is proposed. The approach is based on the Gaussian basis function and the Regularized Hankel's function. The study provides the theoretical background of the newly proposed approach in detail. By expanding the current density on the surface with the summation of Gaussian functions and approximating the Hankel function with regularization leads to having a simpler, compact, and novel approach to investigate the behavior of the electromagnetic field in the vicinity of the obstacles. Also, the numerical results including the comparison with the other methods are provided. The outcomes reveal that the proposed method can be employed for such a class of diffraction problems to solve the problem, numerically.

Numerical experiments have been used to study the properties of reactive fields that form the centers of radiation of the traveling wave field outside the region where real sources are located. It is shown that such reactive fields have a complex vortex character and a high amplitude compared to the traveling wave field. By analytical continuation of the far field in the opposite direction, using the functions of converging waves, it is shown that an external observer can see only the center of the field radiation, but not the reactive field that creates it or real sources. Several examples of the formation of the center of radiation of the traveling wave field outside the region of location of real sources are considered

A NEW NUMERICAL APPROACH TO ELECTROMAGNETIC EIGENVALUE PROBLEM AND WAVE SCATTERING BY CONDUCTING COMPLEX-SHAPED GEOMETRIES: GAUSSIAN BASIS AND REGULARIZED HANKEL FUNCTIONS

Vasil Tabatadze[*], Kamil Karaçuha[**], Ömer Faruk Alperen[*] and Revaz Zaridze[***]

[*]Informatics Institute, Istanbul Technical University, Istanbul, Turkey

[**]Department of Electrical Engineering, Istanbul Technical University, Istanbul, Turkey

[***]The Laboratory of Applied Electrodynamics, Tbilisi State University, Tbilisi, Georgia

E-mail: vasilitabatadze@gmail.com

Abstract

In the present study, a new methodology for solving an eigenvalue problem and the two-dimensional E-polarized electromagnetic wave diffraction by the arbitrary shaped perfect electric conducting (PEC) scatterers is proposed. The approach is based on the Gaussian basis function and the Regularized Hankel's function. The study provides the theoretical background of the newly proposed approach in detail. By expanding the current density on the surface with the summation of Gaussian functions and approximating the Hankel function with regularization leads to having a simpler, compact, and novel approach to investigate the behavior of the electromagnetic field in the vicinity of the obstacles. Also, the numerical results including the comparison with the other methods are provided. The outcomes reveal that the proposed method can be employed for such a class of diffraction problems to solve the problem, numerically.

1. INTRODUCTION AND PROBLEM FORMULATION

The numerical and semi-numerical methods in Electromagnetic diffraction problems are rapidly evolving branches after high-performance computers become cheap and easily accessible. There exist many methods which give approximate solutions to the scattering problems with acceptable and manageable accuracy like the Method of Moments, Finite-difference time-domain method, Finite element method, the Method of Auxiliary Sources (MAS), and Orthogonal Polynomials, etc. [1-9]. The Method of Moments gives the possibility to reduce the scattering problem to an integral equation or

coupled set of an integral equation which finally are expressed as the matrix equation. The method of Moments has a singularity problem when the boundary conditions are required on the surface. To avoid the singularity, Method of Moments uses the regularization technic or tries to find an analytical solution for the self-terms in the matrix equation [1-4]. On the other hand, the method of auxiliary sources for example considering the analytical nature of the field at the boundary and by the analytical continuation of the scattered field, the sources are shifted inside or outside of the corresponding surface [5-7]. Then, the singularity problem is resolved. However, the method of auxiliary sources has the problem when the geometry of the scatterer contains the edge or corners, in that case, the scattered field is not analytical on the surface and auxiliary sources cannot be shifted inside [10-12]. That is why in previous works, the corresponding authors made small changes in the original geometries and have smooth surfaces to obtain results with high accuracy. The change at the corners leads to having a deviation between the solution of the geometry with a smooth surface and the original one. The same procedure was followed for finding eigenvalues and eigenfields of the corresponding geometries. In the present study, these two issues are overcome by introducing the Regularized Hankel function [11,12].

The solution of a fairly wide class of physical problems is reduced to the solution of singular integral equations. As a rule, the kernel of the integral equation has a singularity since at zero value of the argument the value of the kernel becomes infinite. This is purely mathematical infinity, and special mathematical methods have been created to solve this problem (regularization method, etc.). But in physics, as you know, there are no quantities with infinite values. And for all other values of the argument, the value of the kernel has a clear physical meaning. The question arises whether it is possible to initially create such a function, which will have a completely adequate physical meaning, including zero values as the argument. In the presented article, such a problem is posed relative to Green's function for a two-dimensional problem.

In this study, the goal is to introduce a new methodology that will give the possibility to solve the two-dimensional diffraction, eigenvalue, and eigenfield problem for arbitrary shape scatterers. The main idea in this approach is that the Hankel function (corresponding to Green's function in two-dimensional space), which represents the

electric field created by the current density due to the Dirac function is replaced by the regularized Hankel function, which corresponds to the Gaussian current density. The regularized function at the far-field is the same as the Hankel function but at a small distance is a different function that does not have a singularity in the center. This gives the ability to put the sources directly on the surface and require the boundary condition in the same points. As a result, we avoid the singularity problem by regularizing the corresponding function. Therefore, the diffraction problem by arbitrary shape scatterers both smooth and the ones with corners or edges can be solved. Previously, such problems with corners cannot be solved with MAS. Mathematically, it has been shown that a function can be expressed approximately in terms of the linear combinations of translations of Gaussian function [13,14]. This fact triggers us to develop a new and approximate solution for two-dimensional E- polarized electromagnetic diffraction problems. Here, the Method of Moments is employed with expanding the current density on the scatterer surface as a summation of the Gaussian function. As a result, an integral equation is obtained to be solved for matrix coefficients evaluation. Here, to avoid repetitive calculation of the same integral, the corresponding integral is calculated only once, then it is directly employed during the computation by using the regularization. Here, the regularized Hankel's function is proposed. The function is represented by analytical expressions with similar behavior for different arguments. This gives the ability to solve the problem faster.

In the following chapter, the formulation of the problem is presented. The theoretical background would be given in detail. Then, the numerical results obtained by the proposed method are provided. Later, the comparison with the other methods is presented. In the end, the conclusion is drawn.

2. FORMULATION OF THE PROBLEM

In this section, a mathematical background is provided in detail. Due to proposing a new approach, the mathematical derivations would be given from the starting point. Here, we consider the two-dimensional electromagnetic diffraction problem by the PEC object with an arbitrary shape. The investigation covers open, closed, and semi-closed surfaces such as strip, cylinder, and semi-closed circular strip, respectively. All objects

are located in a vacuum. As an excitation source, we can use a plane wave or the cylinder source (both in E-polarized case) with time dependency $e^{-i\omega t}$ where $i = \sqrt{-1}$ is the angular frequency and t is time. The electromagnetic field radiated by the sources excites current on the scatterer' s surface [1,3]. In the present study, all objects have an infinite length in z-direction. Therefore, the electric field has only one component perpendicular to the XoY plane and is oriented along Z-axis [2,3]. To find the scattered electric field (E_sc), the induced current on the scatterer is convolved with the corresponding Green's function given in (3). Then, the scattered field is found by (1) [9]:

$$E_{sc}(x,y) = i\omega A = \frac{\omega\mu}{4}\int_{-\infty}^{\infty}\int_{-\infty}^{\infty} J(x',y')H_0^{(1)}(k\sqrt{(x-x')^2+(y-y')^2})dx'dy' \ , \qquad (1)$$

where $H_0^{(1)} -$ is Hankel's function of zero-order and the first kind and corresponds to the Green's function of the equation, (x', y') stands for the source point, $k = 2\pi/\lambda$ is wavenumber and μ stands for the magnetic permeability. To solve (1), there are many methods are developed [1-4]. Here, the Method of Moments (MoM) approach is employed [1,2]. To solve the integral equation given in (1), the current density is expressed as a summation of the basis functions $f_i(x', y')$ with corresponding constant weights given as a_i. Here, N is the number of source points [13,14].

$$J(x',y') = \sum_{i=1}^{N} a_i \, f_i(x_i, y_i, x', y') \qquad (2)$$

where, $f_i(x_i, y_i, x', y') = \sqrt{2}(\alpha k)^2 e^{-(\alpha d k)^2}$ and $d = \sqrt{(x'-x_i)^2+(y'-y_i)^2}$.
Here, d is the distance between the source point (x', y') and the basis function's center location (x_i, y_i). Note that, all Gaussian functions have the same variance and only translation of them is used in the study. The novelty of the study is to employ the Gaussian function as a basis while expressing the current density induced on the scatterer as given in (6) [13,14]. In fact, (x_i, y_i) are N discrete points on the scatterer's surface and α should be calibrated while comparing the results with strict analytical solutions or the numerical solutions with high accuracy. Keep in mind that, with such an approach, Gaussian function decays fast and is negligible beyond the square area $|x' - x_i| >$

$\lambda, |y' - y_i| > \lambda$. Therefore, we can assign a zero value to the basis function outside this square area.

$$f_i(x', y') = \begin{cases} \sqrt{2}(\alpha k)^2 e^{-(\alpha d k)^2}, & |x' - x_i| \le \lambda, |y' - y_i| \le \lambda \\ 0, & |x' - x_i| > \lambda, |y' - y_i| > \lambda \end{cases} \tag{3}$$

where α is the free parameter to be optimized and λ is the free-space wavelength of the incident wave. The details would be given in the numerical part of the present study. Then, if we put the expression (2) into (1), the induced current and corresponding electric fields will be the smooth functions on the surface as :

$$E_{sc}(x, y) = \frac{\omega\mu}{4}\sqrt{2}(\alpha k)^2 \sum_{i=1}^{N} a_i \int_{y_i - 0.5\lambda}^{y_i + 0.5\lambda} \int_{x_i - 0.5\lambda}^{x_i + 0.5\lambda} e^{-(\alpha k\sqrt{(x'-x_i)^2 + (y'-y_i)^2})^2} H_0^{(1)}(k\sqrt{(x - x')^2 + (y - y')^2}) dx' dy' \tag{4}$$

To apply the boundary condition, the total field ($E(x, y)$) should be obtained mathematically. The corresponding field is the sum of the scattered field and the incident field as $E(x, y) = E_{inc}(x, y) + E_{sc}(x, y)$). On the surface of the scatterer, the boundary of the tangential component of the total electric field should be zero. Because the electric field has only one component and this component is tangential to the scatterer. Therefore, the boundary condition becomes $E(x, y)|_\tau = [E_{inc}(x, y) + E_{sc}(x, y)]|_\tau = 0$. The corresponding equation is provided in (5).

$$E_{inc}(x, y)|_\tau = -E_{sc}(x, y)|_\tau \tag{5}$$

where τ is the tangential vector on the surface which is directed in the z-direction due to having an E-polarized incident wave. Then, the integral equation is obtained after (5) is satisfied:

$$E_{inc}(x, y) = -\frac{\omega\mu}{4}\sqrt{2}(\alpha k)^2 \sum_{i=1}^{N} a_i \int_{y_i - 0.5\lambda}^{y_i - 0.5\lambda} \int_{x_i - 0.5\lambda}^{x_i - 0.5\lambda} e^{-\left(\alpha k\sqrt{(x'-x_i)^2 + (y'-y_i)^2}\right)^2} H_0^{(1)}\left(k\sqrt{(x - x')^2 + (y - y')^2}\right) dx' dy' \tag{6}$$

Here, with the point matching technics including N points ($j = 1,2, \dots N$) on the surface of the scatterer, N equations are obtained by boundary condition as given in (7).

$$E_{inc}(x_j, y_j) = -\frac{\omega\mu}{4}\sqrt{2}(\alpha k)^2 \sum_{i=1}^{N} a_i \int_{y_i-0.5\lambda}^{y_i+0.5\lambda} \int_{x_i-0.5\lambda}^{x_i+0.5\lambda} e^{-(\alpha k\sqrt{(x'-x_i)^2+(y'-y_i)^2})^2} H_0^{(1)}(k\sqrt{(x_j-x')^2+(y_j-y')^2})dx'dy' \tag{7}$$

We can express the corresponding equations as a matrix equation below:

$$Z_{ij} * a_i = B_j \tag{8}$$

where

$$B_j = E_{inc}(x_j, y_j),$$

$$Z_{ij} = -\frac{\omega\mu}{4}\sqrt{2}(\alpha k)^2 \int_{y_i-0.5\lambda}^{y_i+0.5\lambda} \int_{x_i-0.5\lambda}^{x_i+0.5\lambda} e^{-\left(\alpha k\sqrt{(x'-x_i)^2+(y'-y_i)^2}\right)^2} H_0^{(1)}\left(k\sqrt{\left(x_j-x'\right)^2+\left(y_j-y'\right)^2}\right)dx'dy'.$$

Here, (x_i, y_i) are the points where the source is located and double integral is taken around this point.

After finding unknowns by inversion, the current density can be obtained by (2). Similarly, the scattered Electric field can be found with (4). It is clear that for each (x_i, y_i) in the double integral above, the value of the integral would be the same since $e^{-(\alpha k\sqrt{(x'-x_i)^2+(y'-y_i)^2})^2}$ is constant because the integration is taken around (x_i, y_i). Therefore, we can simplify the integral by taking the integration range around the center of the reference frame and the integral denote as regularized Hankel function as (9).

$$RH(x, y) = \int_{-0.5\lambda}^{0.5\lambda}\int_{-0.5\lambda}^{0.5\lambda} e^{-\left(\alpha k\sqrt{(x')^2+(y')^2}\right)^2} H_0^{(1)}(k\sqrt{(x-x')^2+(y-y')^2})dx'dy' \tag{9}$$

Here, RH stands for the abbreviation of the regularized Hankel's Function. While ordinary Hankel's function gives the electric field of the current density represented by Dirac's delta function, the regularized one represents the electric field of the current density represented by the Gaussian function. It should be noted that Dirac's function is the limit case of the Gaussian function. Finally, the scattered field can be expressed as:

$$E_{sc}(x,y) = \frac{\omega}{4}\sum_{i=1}^{N} a_i RH(k\rho) \tag{10}$$

where $\rho = \sqrt{(x-x')^2 + (y-y')^2}$.

To simplify more, (11) is provided.

$$RH(k\rho) = \int_{-0.5\lambda}^{0.5\lambda}\int_{-0.5\lambda}^{0.5\lambda} e^{-\left(\alpha\sqrt{(kx')^2+(ky')^2}\right)^2} H_0^{(1)}(k\rho)d(kx')\,d(ky') \tag{11}$$

To have the faster numerical realization of this method it is better to avoid the calculation of (11), repetitively. This integral has a singular kernel but the value of the integral should be finite because it describes the electric field created with smooth Gaussian current. We can evaluate the integral (11) numerically by using the regularization in the kernel. If we plot this integral for different argument $(k\rho)$, we will get a function which at a big distance behaves like a Hankel's function, and the smaller distance it is a smooth function with no singularity in the center (Fig. 1). That's why we call it the regularized Hankel's function. Because we know the shape of the regularized Hankel's function we can approximate it with some analytical functions. Here, (12) stands for the approximation of (18) with less than 1% error:

$$\widetilde{RH}(k\rho) = \begin{cases} J_0(k\rho) + im\left(A\dfrac{H_0^{(1)}(k\rho)}{\log(0.015k\rho)} - 0.23i\right), if\ k\rho \in (0,2), A = 4.74e^{i\pi\frac{180}{190}} \\ J_0(k\rho) - 1.74i, \qquad k\rho = 0 \\ H_0^{(1)}(k\rho), k\rho \in (2,\infty) \end{cases} \tag{12}$$

where J_0 is the Bessel function with zeroth order.

For $k\rho = 0$, the function has uncertainty, type $\frac{\infty}{\infty}$. It can be resolved. Figure 1(a) shows the plot on which we have both function RH (red) and $\widetilde{RH}$ (blue) for different $k\rho$. Figure 1(b) shows the amplitude of the imaginary part of Hankel's function (red) and the imaginary part of the $\widetilde{RH}$ function (Blue). As we see at the point $k\rho = 2$. $\widetilde{RH}$ the function goes smoothly to the ordinary Hankel's Function. RH does not have a singularity in the point $k\rho = 0$.

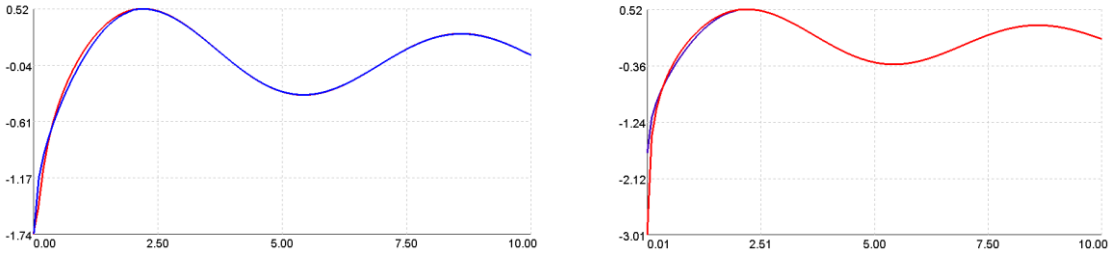

Figure 1. The absolute value of Hankel function and $\widetilde{RH}$ for different $k\rho$

Because the regularized Hankel's function does not have a singularity in the center while requiring the boundary condition on the scatterer's surface, we don't need the regularization technic for the self-terms (when we require boundary condition in the point where the source is located). Therefore, we can put the sources directly on the scatterer's surface. Also, this method works fine with the surface which has sharp corners and edges which is not possible for MAS.

3. RESULTS OF NUMERICAL EXPERIMENTS

In this part, numerical outcomes such as total radar cross-sections, near-field distribution are provided for different scattering and eigenvalue problem geometries. The program package is created and for different geometries, the diffraction and the eigenvalue problems can be obtained with the corresponding program. The α- parameter given in (2) is chosen to be 10 because this value gives the best match between analytical or another numerical approach for different shapes of the scatterer and different frequencies. The closed cavity resonators such as square, H-shaped and asteroid geometries have non-zero Eigen fields at the resonant frequencies [15-17]. To obtain resonance characteristics, an integration over a circular small contour inside the cavities is taken as given in (13). The idea of finding the eigenvalues by solving the scattering problem is proposed in [16,17].

$$R(k) = \int_0^{2\pi} |E_{sc}|^2 d\phi \tag{13}$$

First, let's consider the square. It should be noted that, for square cavities, an analytical solution exists [15]. Fig. 2(a) shows the geometry of the square with the dimension 1X1. Fig. 2(b) shows the frequency characteristics of the corresponding

geometry regarding the wavenumber. Here, the excitation is done by a line source located at (x_inc,y_inc)=(100,0). The sharp resonances corresponding to the eigenvalues of the square are observed.

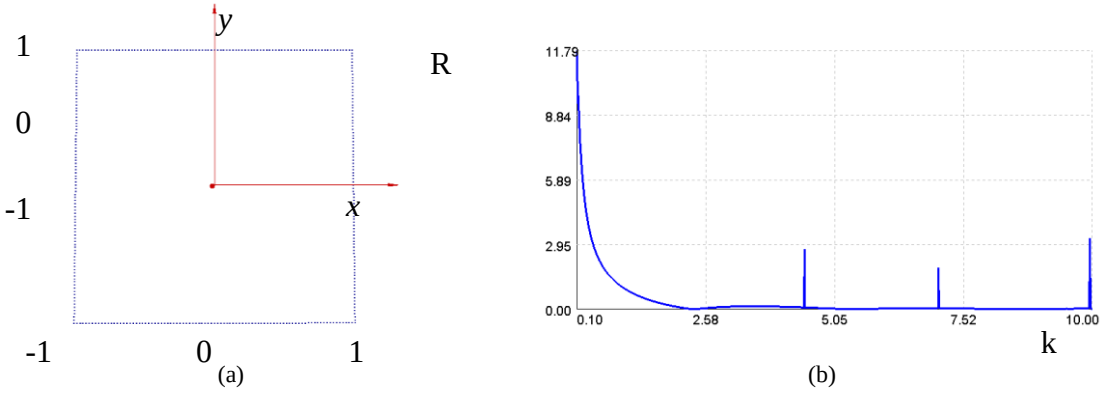

(a) (b)

Figure 2. The geometry of the problem and frequency characteristics of the geometry (b).

At Table 1, the comparison between the analytical and proposed methods for the eigenvalue of the square scatterer is provided. As it is seen, the deviation is less than 0.5% for the first three resonances.

Table 1. Resonance values for the square geometry

Resonances	The Analytical Outcomes for Eigenvalues	Outcomes for Eigenvalues by the proposed approach
First	4.4733	4.4407
Second	7.0234	7.048
Third	9.95	9.9336

Fig. 3(a) shows the near-total field distribution on the first resonance k=4.47 of the square. An electromagnetic wave goes around the square and casts a shadow behind. Inside the square, we see the eigenvalues field. Fig. 3(b) shows the field distribution at the no resonant frequency k=3 where the field inside is practically zero.

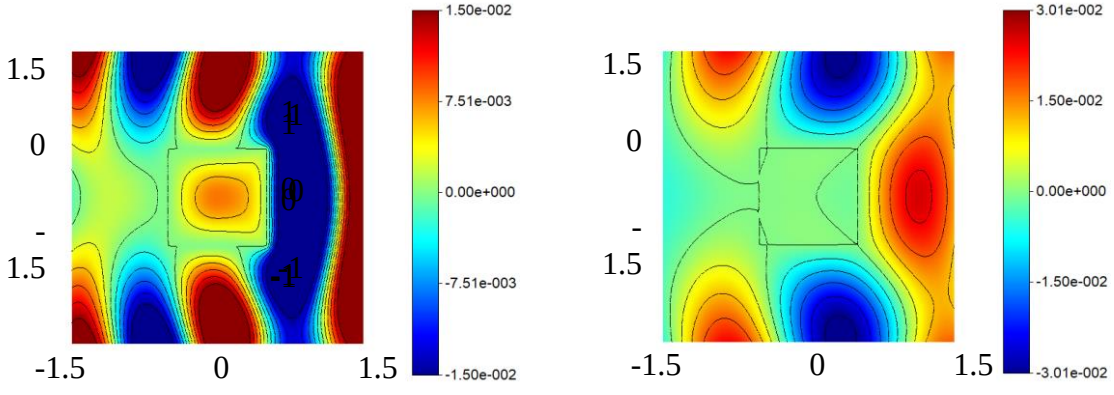

(a) (b)

Figure 3. Total Electric field distributions for square geometry ($k = 4.47$ for (a) and $k = 3$ for (b)).

Let us consider now the H-shaped waveguide, find its resonances, and draw corresponding Eigen fields. Fig. 4(a) shows the geometry of the object. Fig. 4(b) shows the TRCS in the vicinity of the first two resonances.

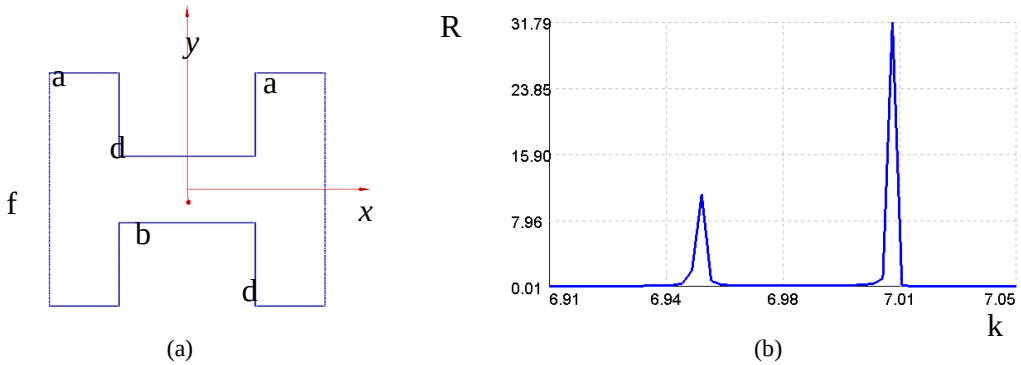

(a) (b)

$(a = 0.4, b = 0.8, d = 0.5, f = 1.4)$

Figure 4. The geometry of the scatterer (a) and the frequency characteristics of the geometry (b).

Fig. 5(a) shows the resonant field distribution at k=6.956 and Fig 5(b) shows the resonant field distribution at k=7.013.

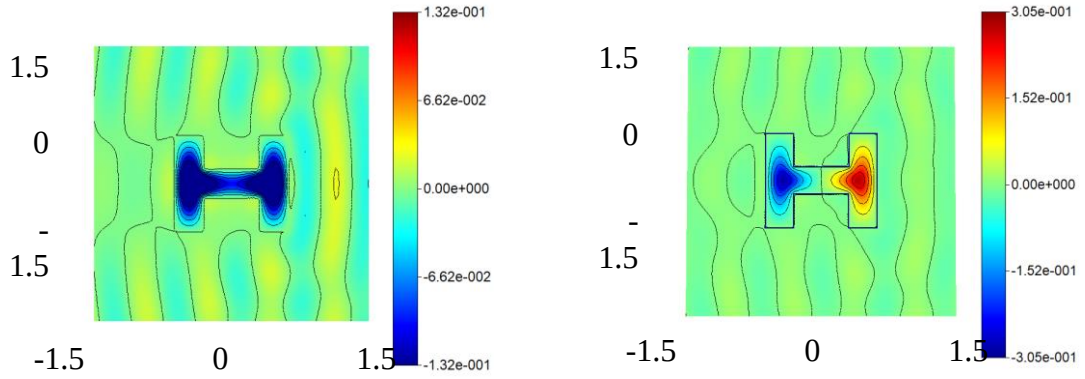

(a) (b)

Figure 5. Total Electric field distributions for H-shaped geometry ($k = 6.956$ for (a) and $k = 7.013$ for (b)).

Fig. 6(a) shows the geometry of the next object which we call 'Asteroid'. Fig. 6(b) shows the TRCS in the vicinity of the first resonance.

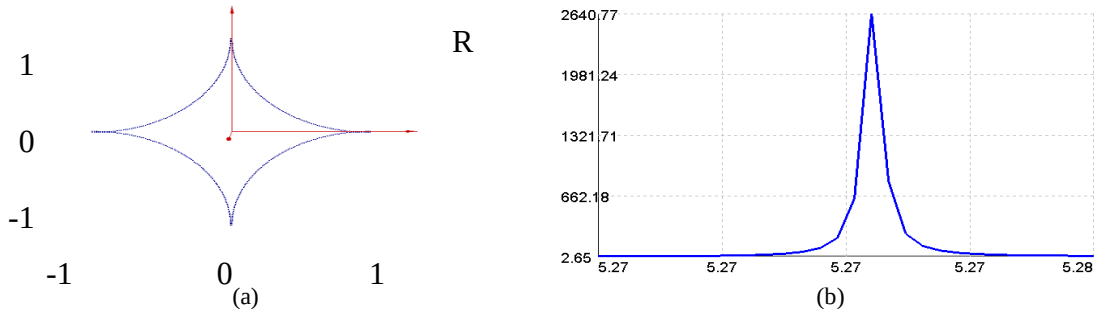

(a) (b)

Figure 6. The geometry of the scatterer (a) and the frequency characteristics of the geometry (b).

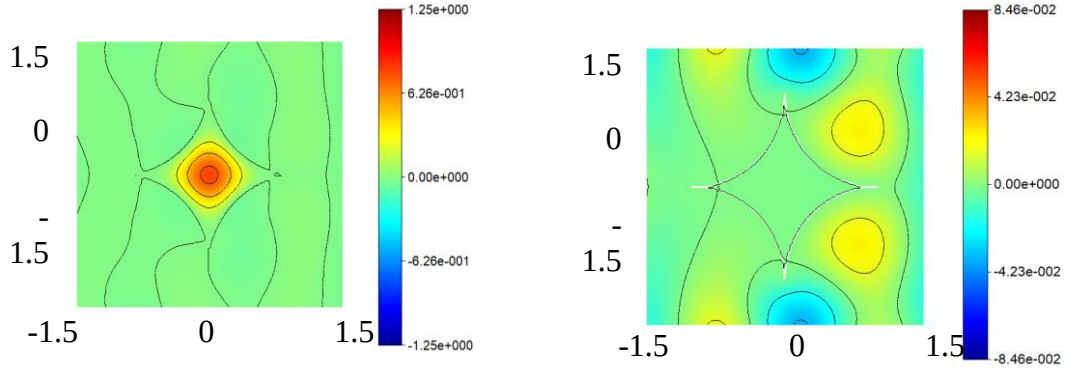

(a) (b)

Figure 7. Total Electric field distributions for asteroid geometry ($k = 5.273$ for (a) and $k = 4$ for (b)).

Fig. 8 shows the total near field distribution at nonresonant frequencies for moon shape, flat-concave lens shape, wedge shape, strip, double side concave lens shape, and the ellipse shape scatterers. Here, r_i, θ_i^{ap}, d_i stand for the radius of the circular geometries, the aperture angle, and length of the strip on the plane, respectively ($i = 1,2$). For the incident line, the source location is denoted with (x_{inc}, y_{inc}). For the wedge geometry given in Fig 8(c), θ corresponds to the angle between two strips.

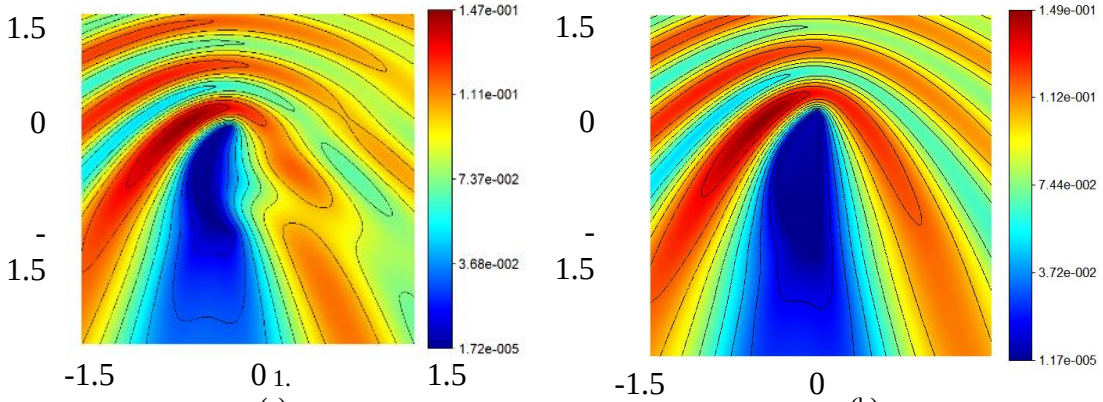

(a)

$k = 4, r_1 = 1, r_2 = 1.5,$
$\theta_1^{ap} = \frac{3\pi}{2.5}, \theta_2^{ap} = \frac{8\pi}{5}, x_{inc} = 0, y_{inc} = 20$

(b)

$k = 4, r = 1.5, d = 2.4,$
$\theta_1^{ap} = \frac{4\pi}{3}, x_{inc} = 0, y_{inc} = 20$

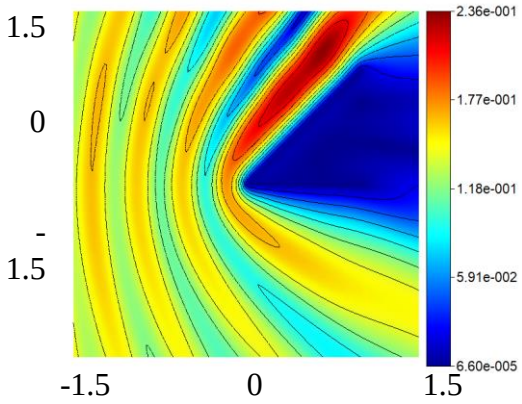

(c)
$k = 4, d_1 = 2, d_2 = 2\sqrt{2},$
$\theta = 45^{\circ} x_{inc} = -10, y_{inc} = 0$

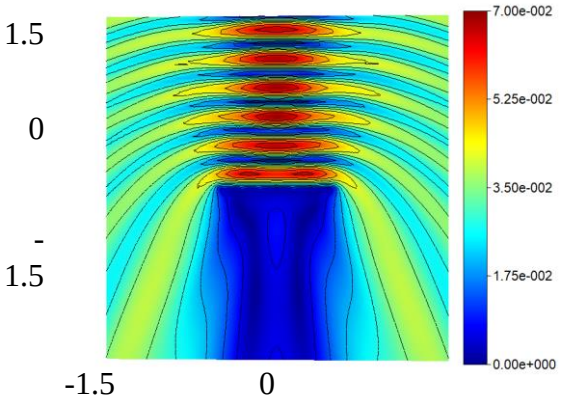

(d)
d- is the size of the strip
$k = 4, d = 2, x_{inc} = 0, y_{inc} = 100$

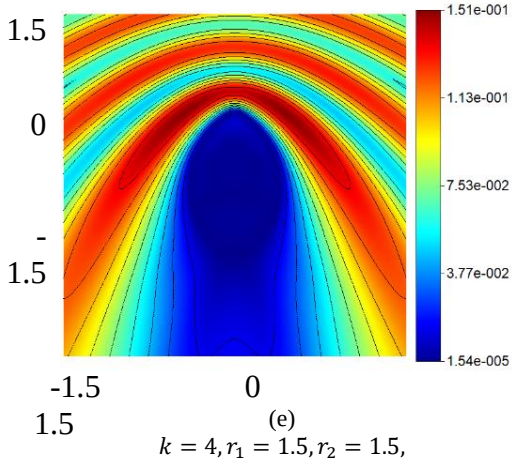

(e)
$k = 4, r_1 = 1.5, r_2 = 1.5,$
$\theta_1^{ap} = \frac{4\pi}{3}, \theta_2^{ap} = \frac{4\pi}{3} x_{inc} = 0, y_{inc} = 20$

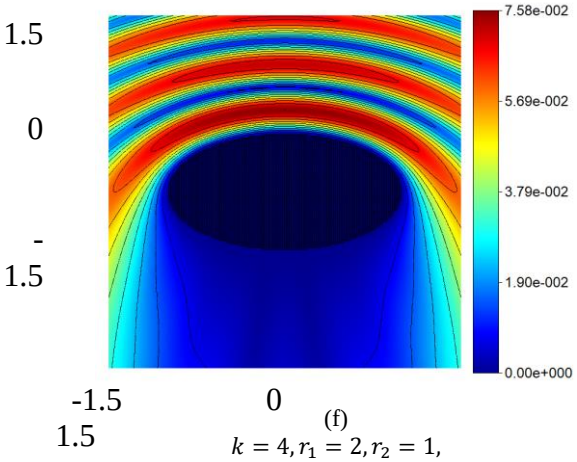

(f)
$k = 4, r_1 = 2, r_2 = 1,$
$\theta_1^{ap} =, \theta_2^{ap} = x_{inc} = 0, y_{inc} = 100$

Figure 8. Total Electric field distributions for (a) moon shape, (b) Plano-convex lens, (c) wedge, (d) strip, (e) convex lens, (f) ellipse.

4. COMPARISON WITH THE OTHER METHODS

Fig. 9 shows the comparison results of the frequency characteristics obtained with the proposed method (red) and the method of orthogonal polynomials (blue) [9]. The comparison is obtained for the diffraction by the PEC circular arc with the radius 1 and the aperture angle of 60 degrees. The source is located in the center. As it is noticed the first resonance coincides regarding the wavenumber and amplitude. The second resonant frequency value is also matched. However, the deviation of amplitude is observed. This can be explained by the fact that as the excitation, in the proposed approach, the regularized Hankel is employed. In contrast, the ordinary Hankel function is used for the other approach.

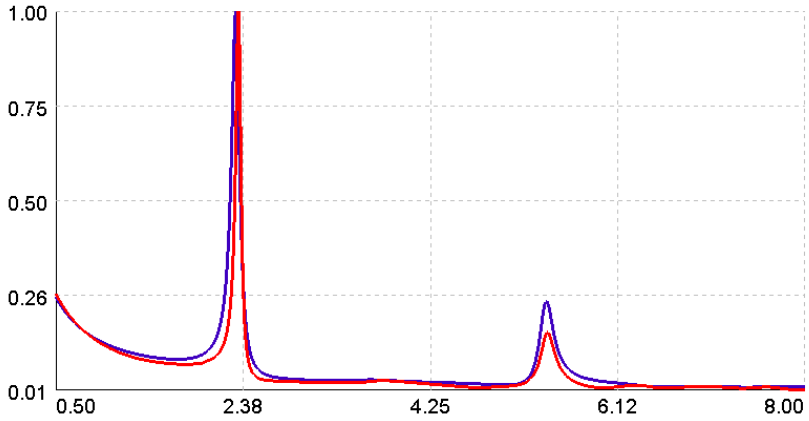

Figure 9. Normalized frequency characteristics of the circular arc by the proposed method (red) and the orthogonal polynomials approach (blue).

Fig. 10 shows both comparisons of the current density and the near field distribution due to the PEC strip with the size 2 at $k = 4$. Here, the source is located at $x_{inc} = 0, y_{inc} = 10$. The red graph is obtained with MoM using pulse basis function and the blue one is obtained with the present method. The deviation in the current density is observed since the regularized Hankel function is employed in the proposed approach. Fig. 10(b) and (c) provide the total near electric field distributions obtained by the proposed and MoM (pulse function, point matching) approaches, respectively.

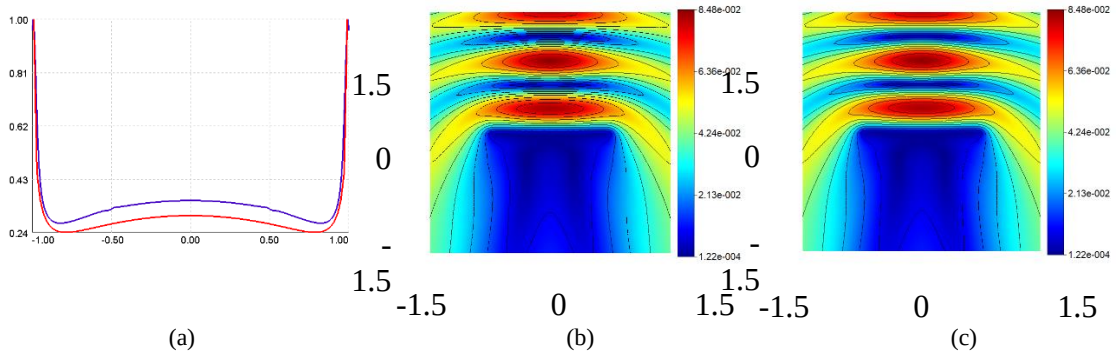

Figure 10. Comparison of two methodologies (MoM and proposed approach) (a) Absolute Value of the Current Densities and Electric Field Distributions by the proposed approach (b) and MoM (c).

5. CONVERGENCE

We also investigated the convergence of our result for the diffraction by the circular PEC arc with radius 1 and the aperture size of 60 degrees. We estimated the

satisfaction of the boundary condition in the point of the arc contour in comparison with the incident field amplitude. Fig. 11 shows the corresponding graph. As we see, by increasing the number of discretization points the graphs approach the zero value. In terms of the incident field amplitude, the boundary condition in the point on the arc is 99.95 % is satisfied when $N = 500$. Also, for the higher frequency, the same procedure is followed and the error in the boundary condition is found 0.09 % for $N = 500$. It should be denoted that, less than 1 percent error can be obtained after $N > 30$.

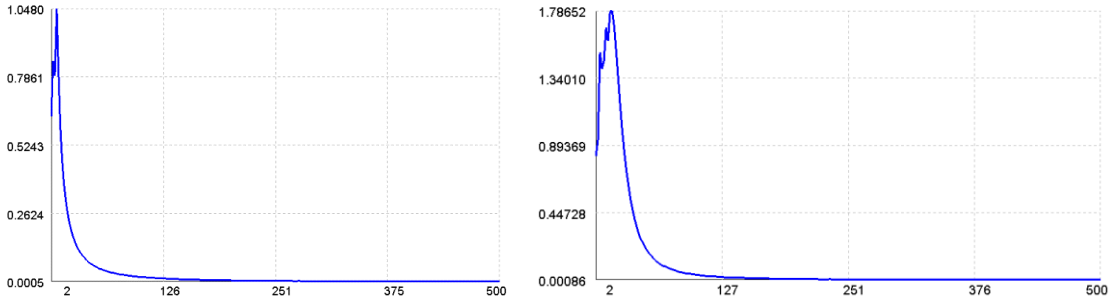

(a) (b)

Figure 11. The error in boundary condition satisfaction (%) versus the collocation points (N) (a) $k = 4$ (b) $k = 8$.

4. CONCLUSION

In this article, a new methodology for the two-dimensional diffraction problem of the E-polarized electromagnetic wave by the arbitrarily-shaped perfect electric conducting scatterer is presented. Gaussian basis function is introduced for the current density representation and the Regularized Hankel's function is defined which gives the ability to put the secondary sources directly on the scatterer. The present study has the advantage in comparison with other methods such as MoM and MAS since the boundary condition is satisfied in the same points where the secondary sources are located. As a result, the singularity problem is avoided. Such an approach gives the ability to solve the diffraction problem by an arbitrary shape scatterer consisting of both smooth parts as well as the corners and edges. The comparison with other methods reveals that the gives highly accurate results are obtained by the proposed method. Furthermore, the introduction of the Gaussian function as the basis function gives the ability to extend the proposed approach for two-dimensional H-polarization and also three-dimensional cases.

REFERENCES

[1] WC. Gibson, “The method of moments in electromagnetics”, CRC Press; 2014.

[2] RF. Harrington, “Field computation by moment methods”, Wiley-IEEE Press; 1993.

[3] CA. Balanis, “Advanced engineering electromagnetics”, John Wiley & Sons; 2012.

[4] PY. Ufimtsev, G. Apaydin, “Bistatic scattering at soft–hard strips and plates: method of moments (MoM), theory of edge diffraction (TED), and physical theory of diffraction (PTD) analysis”, IET Microwaves, Antennas Propag. 2020;14:1117–1123

[5] FG. Bogdanov, DD. Karkashadze, RS. Zaridze, “The method of auxiliary sources in electromagnetic scattering problems”, Gen Multipole Tech Electromagn Light Scatt. Elsevier; 1999. p. 143–172.

[6] R. Zaridze, G. Bit-Babik, K. Tavzarashvili, et al. “The method of auxiliary sources (MAS)—Solution of propagation, diffraction and inverse problems using MAS”, Appl Comput Electromagn. Springer; 2000. p. 33–45.

[7] IM. Petoev, VA. Tabatadze, RS. Zaridze, “The method of auxiliary sources applied to problems of electromagnetic wave diffraction by certain metal-dielectric structures”, J Commun Technol Electron. 2013;58:404–416.

[8] V. Tabatadze, K. Karaçuha, EI. Veliyev, “The solution of the plane wave diffraction problem by two strips with different fractional boundary conditions”, J Electromagn Waves Appl [Internet]. 2020;34:881–893. Available from: https://doi.org/10.1080/09205071.2020.1759461.

[9] K. Karaçuha, “General approach to the line source electromagnetic scattering by a circular strip: Both E-and H-polarisation cases”, IET Microwaves, Antennas Propag. 2021;15:1721–1734.

[10] RS. Zaridze, R. Jobava, G. Bit-Babik, et al. “The method of auxiliary sources and scattered field singularities (caustics)”, J Electromagn waves Appl. 1998;12:1491–1507.

[11] V. Kopaleishvili, R. Zaridze, “Diffraction on a finite system of cylinders”, Radiotech. Electron. 1972;11.

[12] R. Zaridze, D. Karkashadze, G. Ahvlediani, J. Khatiashvili, “Investigation of Possibilities of the Method of Auxiliary Sources in Solution of two-dimensional Electrodynamics Problems”, Radiotech. Electron. 1981 26(2).

[13] C. Calcaterra, A. Boldt. “Approximating with Gaussians”, arXiv Prepr arXiv08053795. 2008

[14] C. Calcaterra. “Linear Combinations of Gaussians with a Single Variance are dense in L2”, Proc World Congr Eng. 2008.

[15] RF. Harrington, “Time-harmonic electromagnetic fields”, Society A and P, Society MT and T.. McGraw-Hill New York; 1961.

[16] I. Petoev, V. Tabatadze, R. Zaridze, "The method of auxiliary sources for eigenfrequencies and Eigen fields determination", 2015 XXth IEEE Int Semin Direct Inverse Probl Electromagn Acoust Wave Theory. IEEE; 2015. p. 13–17.

[17] R. Zaridze, D. Kakulia, K. Tavzarashvili, et al. "Determination of eigenvalues of the object using the method of auxiliary sources (MAS)", DIPED-2001 Proc 6th Int Seminar Direct Inverse Probl Electromagn Acoust Wave Theory (IEEE Cat No 01TH8554). IEEE; 2001. p. 183–186.

INVESTIGATION OF SOME PROPERTIES OF REACTIVE FIELDS

I. Darsavelidze*, R. Zaridze*, J. Manjgaladze*

* Tbilisi State University (TSU)
Georgia, 0128 Tbilisi, Chavchavadze Ave 3

E-mail: ivane.darsavelidze@tsu.ge

Abstract

Numerical experiments have been used to study the properties of reactive fields that form the centers of radiation of the traveling wave field outside the region where real sources are located. It is shown that such reactive fields have a complex vortex character and a high amplitude compared to the traveling wave field. By analytical continuation of the far field in the opposite direction, using the functions of converging waves, it is shown that an external observer can see only the center of the field radiation, but not the reactive field that creates it or real sources. Several examples of the formation of the center of radiation of the traveling wave field outside the region of location of real sources are considered.

1. INTRODUCTION

The article is devoted to the observed in numerical experiments phenomenon of the emergence of a center of radiation (singularity) of the far field, when real sources are located in another area. We call the far-field singularities the regions of its analytical continuation, with dimensions of the order of the wavelength, which are the centers of equal phases and the centers of radiation of this field. In some cases this phenomenon takes place if the values of the amplitudes and phases of real sources are properly selected. Studies show that this produces high reactive fields with a special vortex structure, which form this singularity. The purpose of this work is to study the properties of such reactive fields using a number of examples.

As is known, the reactive field is present in the near zone of any electromagnetic emitter (or scatterer) and has the character of a non-propagating standing wave. The size of the area occupied by it depends on the quality of the antenna matching with the external space. With good matching, these areas are minimal. The amplitude of the

reactive field, with increasing distance from the emitter, rapidly decreases (inversely proportional to the cube and the square of this distance), in far zone is equal to zero and therefore, information about it is not contained in the far zone.

To be convinced of the statement above, lets discuss an approximate expression for the field of a radiator (scatterer) with a smooth surface, which can be represented as the sum of the fields of elementary radiators (for example, Hertz dipoles [1]) on this surface:

$$\vec{E} \approx \sum_{n=1}^{N} a_n \exp\left(ikR_n\right)\left(1/R_n^3 - ik/R_n^2\right)\left[3\vec{R}_{n0}\left(\vec{R}_{n0}\cdot\vec{p}_n\right) - \vec{p}_n\right]$$

$$+\sum_{n=1}^{N} a_n k^2 \exp\left(ikR_n\right)\left(1/R_n\right)\left(\left(\vec{R}_{n0}\times\vec{p}_n\right)\times\vec{R}_{n0}\right). \qquad (1)$$

Here R_n and $\vec{R}_{n0}$, respectively, the distance and unit vector from the *n* - th dipole to a variable point in space, a_n and $\vec{p}_n$, accordingly, the complex amplitude and polarization vector of the *n* - th dipole, k wavenumber, *N* is the total number of sources. We present the expression in this form in order to separate the reactive part of the field near zone and Fresnel zone (the first sum) from the part propagating into the far zone (the second sum). In the far zone (for all $R_n >> \lambda$ the reactive field cannot participate and the approximate equality is written

$$\vec{E}\big|_{r>>\lambda} \approx \sum_{n=1}^{N} a_n k^2 \exp\left(ikR_n\right)\left(1/R_n\right)\left(\left(\vec{R}_{n0}\times\vec{p}_n\right)\times\vec{R}_{n0}\right).$$

It should be noted that in the problems of antenna synthesis (to which we have devoted works [2-7]), the far field is initially set in the form

$$\vec{E}\big|_{r>>\lambda} \approx \frac{\exp\left(ikR\right)}{R}\vec{F}\left(\vartheta,\varphi\right),$$

where R is some averaged value of all R_n, and $\vec{F}\left(\vartheta,\varphi\right)$ the complex vector radiation pattern, i.e, the reactive field is not taken into account in advance. It is known that when solving synthesis problems, the aperture of the target antenna is selected in advance, and then currents are sought on this surface, providing the required diagram. In the case of selecting a different surface of the antenna, the currents providing the same diagram are

different. In this case, only the structure of the reactive field changes. Based on this, it can be argued that the same far field can be obtained by different distributions of sources (surfaces and currents) in the near zone.

This statement does not contradict the uniqueness of the analytic continuation of the far field. It follows from the fact that in the near zone of the analytical continuation there is no information about the reactive field, since it does not initially participate in the far zone, from where this continuation is constructed. That is why, in [2-7], it was proposed to solve the problem of antenna synthesis by constructing an analytical continuation of a given far field into the near zone and finding its singularities. It was argued that by placing the sources at the found points of the far-field singularities, we will get the most optimal antenna, that is, with the smallest values of the reactive field. It was shown that for other distributions of sources that also provide a given far field, the dimensions of the reactive field and its amplitudes have higher values.

The analytical properties of a traveling wave are well studied, as it is a carrier of information, it is precisely because of that, in most cases, studying it was of practical interest. Perhaps for this reason, the properties of the reactive fields themselves have not yet been deeply studied, despite the presence of a number of recent works in this direction (for example [8-10]). This work is devoted to the study of some properties of reactive fields, which are mathematically described by the first term of sum in (1). On the example of the addition theorem for cylindrical functions, as well as on a number of other examples, it is shown that high reactive fields are capable of creating singularities of the analytical field of a traveling wave outside the location of its real sources. The goal of this work is to study the properties of such reactive fields. For simplicity of calculations and visualization of field patterns, mainly two-dimensional cases are considered. The case of a three-dimensional field is considered at the end. Numerical calculations are carried out using the Method of Auxiliary Sources (MAS) [11-18]. It is assumed that the time factor has the form $\exp(-i\omega t)$.

2. THEORETICAL PART

As an initial example of the formation of a center of far-field radiation by sources outside the region of real sources, let's discuss the addition theorem for cylindrical functions and describe its physical meaning.

Consider the series

$$\sum_{n=-\infty}^{+\infty} J_n\left(k\rho_0\right) H_n^{(1)}\left(k\rho\right) \exp\left(-in\varphi\right), \tag{2}$$

where $\rho_0 = const$, $0 \le \rho < \infty$, $0 \le \varphi < 2\pi$. According to the addition theorem, everywhere outside the circle of radius ρ_0, that is, for $\rho > \rho_0$ (Figure 1), this series converges and the equality

$$\sum_{n=-\infty}^{+\infty} J_n\left(k\rho_0\right) H_n^{(1)}\left(k\rho\right) \exp\left(-in\varphi\right) = H_0^{(1)}\left(k\left|\vec{\rho} - \vec{\rho}_0\right|\right). \tag{3}$$

In other words, outside the circle, this series has a well-defined physical meaning of the field of a point source of the type $H_0^{(1)}$ centered at point O_1. As for the inner region ($\rho < \rho_0$), in it the series (2) diverges (studies have shown that only the imaginary part diverges) and it cannot be identified with the physical field.

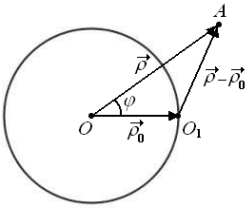

Figure 1. The geometry of the summation

However, the situation will change if we restrict ourselves to a finite sum and consider the approximate equality

$$\sum_{n=-N}^{+N} J_n\left(k\rho_0\right) H_n^{(1)}\left(k\rho\right) \exp\left(-in\varphi\right) \approx H_0^{(1)}\left(k\left|\vec{\rho} - \vec{\rho}_0\right|\right). \tag{4}$$

Calculations show that for a given value of $k\rho_0$, it is possible to choose *N* that provides sufficient accuracy. Since the left side of (4) is a finite sum, and each of its terms satisfies the wave equation, it acquires a quite definite physical meaning of the

wave field inside the circle. Moreover, N is the number of real sources of the type of $H_n^{(1)}(k\rho)$ of this field.

The field is emitted by these sources from the origin, but for an observer in the traveling wave zone, the radiation comes from point O_1, where there is actually no real source. For this reason, we also call the point O_1 an imaginary source. At the point O_1 there is a singularity of the analytic continuation of the external field. The observer cannot see real sources at the origin of coordinates, since they create only an internal reactive field, which does not propagate. Said above is confirmed by an example of constructing an analytical continuation of the far field into the near zone to singularities, at $k\rho_0 = 4$ (Figure 2), by the method proposed in [2 and 18]. Only the center of far-field radiation is visible, which, with an increase in N in the sum (4), gradually shifts from point O to point O_1.

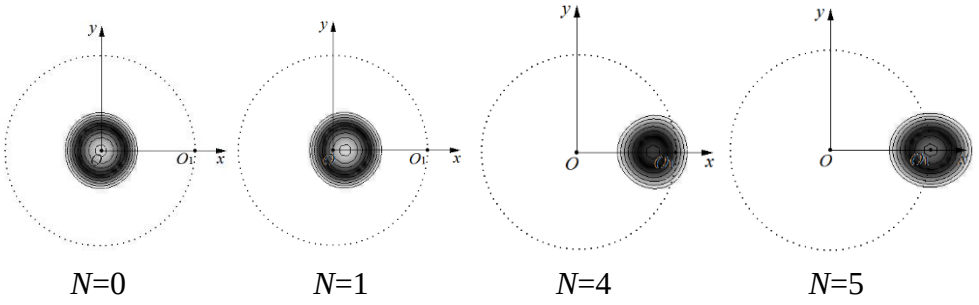

Figure 2. Displacement of the center of radiation of the analytical continuation of the far field, with increasing *N*.

Figure 3a shows curves of equal field phases in the left-hand side of (4), for $k\rho_0 = 5$ and $N = 13$. It can be seen that outside the circle it coincides with good accuracy with the field of a point source centered at point O_1. Analysis of the internal field shows that it has the character of a "breathing", non-propagating standing wave. During one period, the Poynting vector changes direction several times, which is typical for a reactive field. It should be noted that the change in the direction of this vector for different interior points does not occur simultaneously. As a result, in the region of the reactive field, regions appear in which countercurrents of energy arise. This explains the appearance of vortices of force lines of Poynting vectors in the inner region (Figure 3b). Adding even

one next source significantly changes the nature of the redistribution of energies between them, and as a result, the values and general picture of the reactive field change significantly. In particular, new areas with vortices appear. This is the manifestation of the divergence of series (2) in the region of the reactive field. In this case, the accuracy of determining the far field increases.

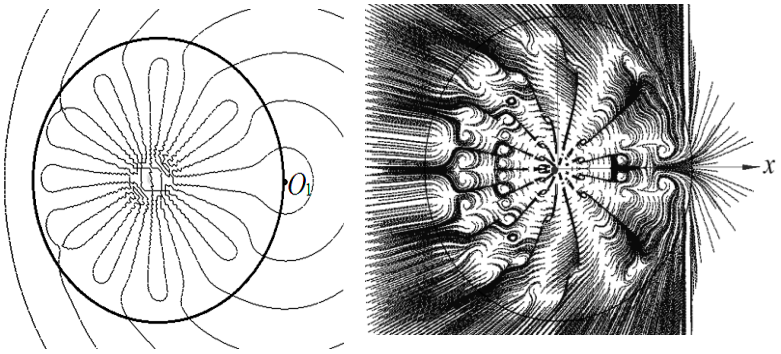

a) b)

Figure 3. The field, when N =13 and $k\rho_0$=5: a) the equal phase curves, b) the Poynting vector field lines.

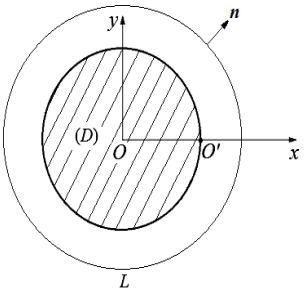

Figure 4. The inner area and outer contour.

For a more detailed study of the energy picture of the field

$$\vec{E}(\vec{\rho}) = \sum_{n=-N}^{+N} J_n(k\rho_0) H_n^{(1)}(k\rho) \exp(-in\varphi)\vec{z}\,,$$

the dependences of the internal energy U (in the region (D)) and the energy flux W through the external closed loop are studied, for some values $k\rho_0$ on the N (Figure 4, 5a and 5b):

$$U = \frac{1}{2}\iint_{(D)} \left(\varepsilon_0 \left|\vec{E}(\vec{\rho})\right|^2 + \mu_0 \left|\vec{H}(\vec{\rho})\right|^2\right) dxdy\,,\; W = \frac{1}{2}\oint_L \mathrm{Re}\left(\vec{E}(\vec{\rho}) \times \vec{H}^*(\vec{\rho})\right)\vec{n}dL\,.$$

Here $\vec{H}(\vec{\rho})$ is the magnetic component of the field, $\vec{n}$ the outer normal to the contour L. With an increase in N, the energy flux approaches the corresponding value for the field of a point source. The internal energy of the reactive field, however, greatly increases. Attention should also be paid to the value of the order of 10^{15}, while for the energy flow we have the order of 10^{-3}.

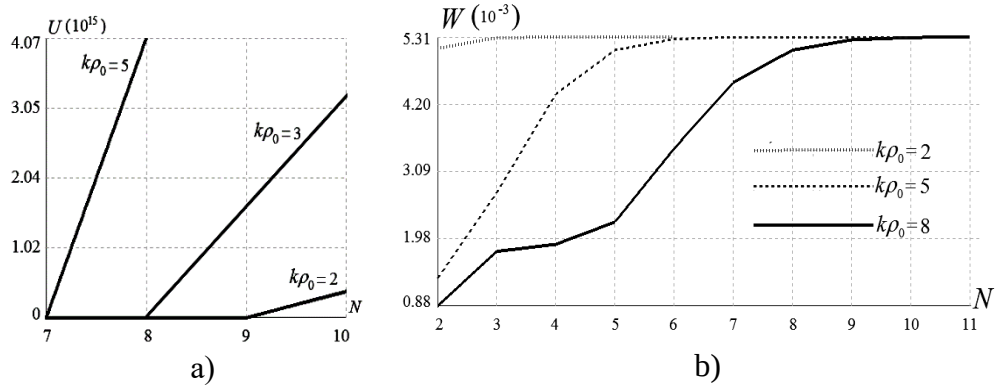

Figure 5. Dependences on *N* for: a) energy flow through the outer contour, b) internal energy.

It is interesting that the series composed of the coefficients $J_m(k\rho_0)$ of the addition theorem converges to one ([19] see 8.512 1), that is, to the amplitude of the imaginary source equal to unity:

$$\sum_{n=-\infty}^{\infty} J_n(k\rho_0) = J_0(k\rho_0) + \sum_{n=1}^{\infty}\left[J_n(k\rho_0) + J_{-n}(k\rho_0)\right] = J_0(k\rho_0) + 2\sum_{n=1}^{\infty} J_{2n}(k\rho_0) = 1.$$

It should be noted that the consideration of sources of the high order type $H_n^{(1)}$ is not the only one for obtaining the field of one source at point O_1. Below, on several examples, it is shown that by various distributions of sources of type $H_0^{(1)}$, it is also possible to obtain such a field.

Let's rewrite (4) in an equivalent form:

$$J_0(k\rho_0)H_0^{(1)}(k\rho) + \sum_{n=1}^{N} 2J_n(k\rho_0)H_n^{(1)}(k\rho)\cos n\varphi \approx H_0^{(1)}\left(k\left|\vec{\rho} - \vec{\rho}_0\right|\right).$$

We have studied the diagrams and behavior of the fields of individual members, i.e.

$$2J_n(k\rho_0)H_n^{(1)}(k\rho)\cos n\varphi. \qquad (5)$$

Figure 6 shows the radiation patterns of these fields for $n = 1, 2, 3, 4$ and $k\rho_0 = 2$. The number of petals in these diagrams is 2*n*.

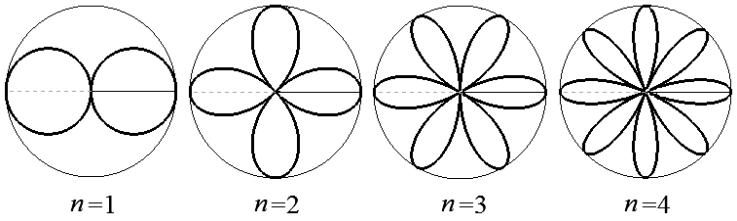

Figure 6. Field radiation pattern when

It can be shown that each of these fields, for the corresponding *n*, can also be obtained by uniformly distributing $2n$ $H_0^{(1)}$ type point sources along a circle of some radius $\Delta\rho_n$, determined from the condition

$$k\Delta\rho_n = \sqrt[n]{2^{n-1}\left|J_n\left(k\rho_0\right)\right|(n-1)!}\,.$$

Moreover, each source must radiate in antiphase with the neighboring one.

For the case $k\rho_0 = 2$, we have the following first four values of $k\Delta\rho_n$: 0.58, 0.84, 1.02, 1.14

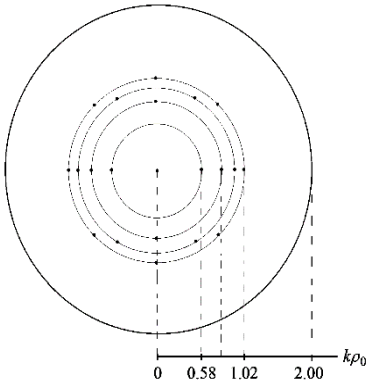

Figure 7. Sources distribution along the circle.

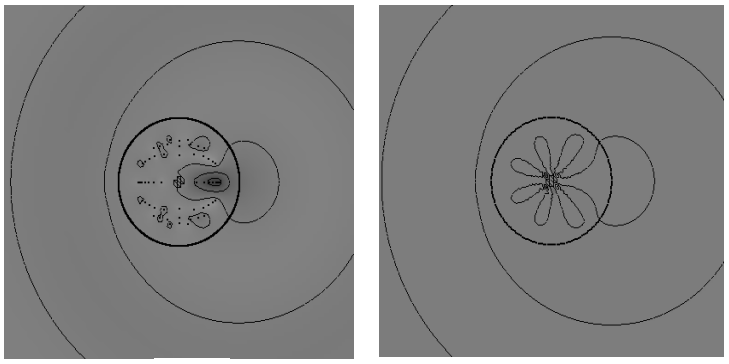

a) b)

Figure 8. Comparison of fields for *N*=4: a) the case of sources on circles, b) the case of the summation theorem.

Figure 7 shows the corresponding circles, with sources of the type $H_0^{(1)}$ distributed along them. Figures 8a) and 8b) show a comparison of the source fields in figure 7, with the addition theorem field. It is seen that in the outer region these fields coincide with the field: $H_0^{(1)}\left(k\left|\vec{\rho}-\vec{\rho}_0\right|\right)$, but their reactive fields are different. This confirms that the same far field can be obtained by different source distributions and only the structure of the reactive field depends on the nature of the distribution.

Let us consider a more general case when the field $H_0^{(1)}\left(k\left|\vec{\rho}-\vec{\rho}_0\right|\right)$ should be obtained by N number of sources of the type $H_0^{(1)}$ distributed on some contour l (Figure 9a). The total field of such sources has the form

$$\sum_{n=1}^{N} a_n H_0^{(1)}\left(k\left|\vec{\rho}-\vec{\rho}_n\right|\right),\ \vec{\rho}_n \in l\,. \tag{6}$$

The coefficients a_n have the meaning of the complex amplitudes (currents) of these sources and are determined from the condition of equality of fields (6) and $H_0^{(1)}\left(k\left|\vec{\rho}-\vec{\rho}_0\right|\right)$ on the $\tilde{l}$:

$$\sum_{n=1}^{N} a_n H_0^{(1)}\left(k\left|\vec{\tilde{\rho}}_m-\vec{\rho}_n\right|\right)=H_0^{(1)}\left(k\left|\vec{\tilde{\rho}}_m-\vec{\rho}_0\right|\right),\ \vec{\tilde{r}}_m \in \tilde{l}\ ,\ m=1,2,...,N\ . \tag{7}$$

Expression (7) is a system of linear algebraic equations for the coefficients a_n, the solution of which is carried out on a computer.

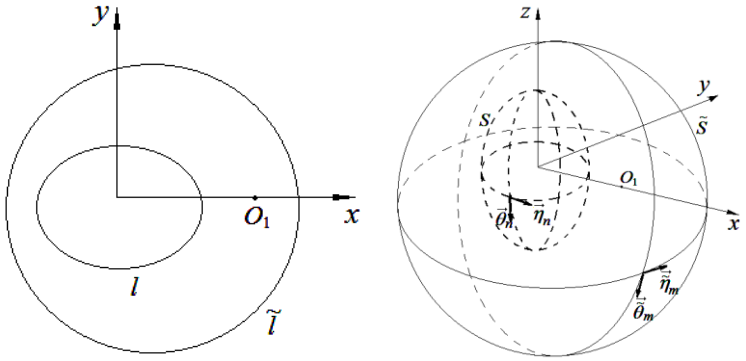

a) b)

Figure 9. Obtaining the imaginary source using MAS: a) two-dimensional case, b) three-dimensional case.

In the three-dimensional case, the problem is reduced to obtaining the Hertz dipole field centered at the point O_1

$$\vec{E}_0\left(\vec{r},\vec{r}_0\right)=\left(4\pi\varepsilon_0\right)^{-1}\exp\left(ikR'\right)$$
$$\times\left\{\left(1/R^3-ik/R^2\right)\left[3\vec{R}_0\left(\vec{R}_0\cdot\vec{p}\right)-\vec{p}\right]-\left(k^2/R\right)\vec{R}_0\times\left(\vec{R}_0\times\vec{p}\right)\right\} \tag{8}$$

a set of *N* auxiliary sources on some smooth surface *S* (Figure 9b). Here $R = |\vec{r} - \vec{r}_0|$ and $\vec{R}_0 = \vec{R}/R$. The auxiliary source consists of two mutually perpendicularly oriented Hertz dipoles with unknown complex amplitudes a_n and b_n, polarized along the tangent vectors $\vec{\eta}_n$ and $\vec{\vartheta}_n$ to the surface *S*. The total field of auxiliary sources is written as:

$$\vec{E}(\vec{r}) = (4\pi\varepsilon_0)^{-1} \sum_{n=1}^{N} \exp(ikR_n)\left(1/R_n^3 - ik/R_n^2\right)\left[3\vec{R}_{n0}\left(\vec{R}_{n0}\cdot\vec{p}_n\right) - \vec{p}_n\right]$$

$$-k^2 (4\pi\varepsilon_0)^{-1} \sum_{n=1}^{N} \left[\exp(ikR_n)/R_n\right]\vec{R}_{n0}\times\left(\vec{R}_{n0}\times\vec{p}_n\right), \qquad (9)$$

where: $\vec{p}_n = a_n\vec{\eta}_n + b_n\vec{\vartheta}_n$, $\vec{R}_n = \vec{r} - \vec{r}_n$, $\vec{R}_{n0} = \vec{R}_n/R_n$, $\vec{r}_n \in S$. The unknown coefficients a_n and b_n are determined from the condition of equality of fields (8) and (9) along two mutually perpendicular tangent vectors $\vec{\tilde{\eta}}_m$ and $\vec{\tilde{\vartheta}}_m$ on the surface:

$$\vec{E}\left(\vec{\tilde{r}}_m\right)\cdot\vec{\tilde{\eta}}_m = \vec{E}_0\left(\vec{\tilde{r}}_m, \vec{r}_0\right)\cdot\vec{\tilde{\eta}}_m,\ \vec{E}\left(\vec{\tilde{r}}_m\right)\cdot\vec{\tilde{\vartheta}}_m = \vec{E}_0\left(\vec{\tilde{r}}_m, \vec{r}_0\right)\cdot\vec{\tilde{\vartheta}}_m,$$

where $\vec{\tilde{r}}_m \in \tilde{S}$ and *m* = 1,2, ..., *N*. It is convenient to construct the surface $\tilde{S}$ in the zone of the traveling wave, which will make it possible to disregard the reactive part of the fields (8) and (9). Below, we describe the results of some numerical experiments on obtaining imaginary radiation centers outside the region where real sources are located. It is assumed that the radiation of each such source does not affect the other sources, that is, they are "Untied". In practice, obtaining such untied sources is quite difficult, but in some cases it is possible. Therefore, we assume that the results described below can be implemented in practice.

3. NUMERICAL RESULTS

3.1. The case of distribution of sources on a circle

Consider $H_0^{(1)}$ type 15 auxiliary sources distributed along a circle centered at the origin and radius R, with $kR = 2$. By the method described above, the values of their complex amplitudes were found, which ensure the formation of the field of a point source of unit amplitude, centered at point O_1.

Figure 10a) shows the nature of the curves of equal phases of the field near the auxiliary contour. Inside the circle $k\rho_0 = 4$, which is the "boundary", the field has a reactive character, with high amplitudes, in comparison with the external field. This is confirmed by animation and analysis of the internal field. In this case, a phase shift between the electric and magnetic components is observed, close to $\pi/2$. The radius of the circle $\tilde{R}$ on which the condition (7) of equality of fields is required is defined as $k\tilde{R} = 10$.

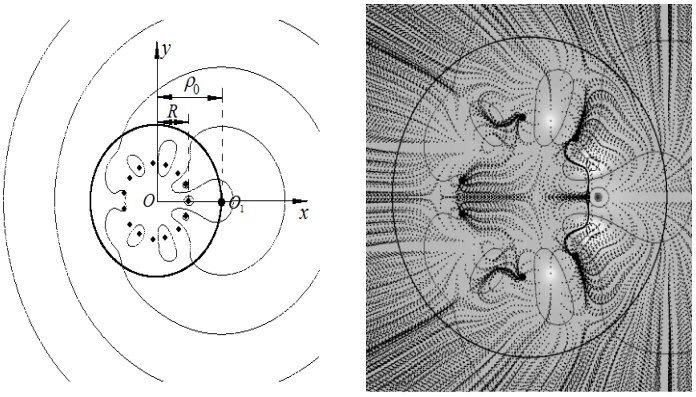

a) b)

Figure 10. Obtaining the imaginary source by 15 sources on the circle: a) the inner and outer fields, b) the Poynting vector lines in the inner area.

Figure 10b) shows an enlarged fragment supplemented by the Poynting vector field lines. The presence of vortices of these lines is also seen here. The figure 11a) and 11b) show the absolute values and phases of the amplitudes of the auxiliary sources. According to figure 11a), the source close to point O_1 (numbered 8) has the maximum amplitude.

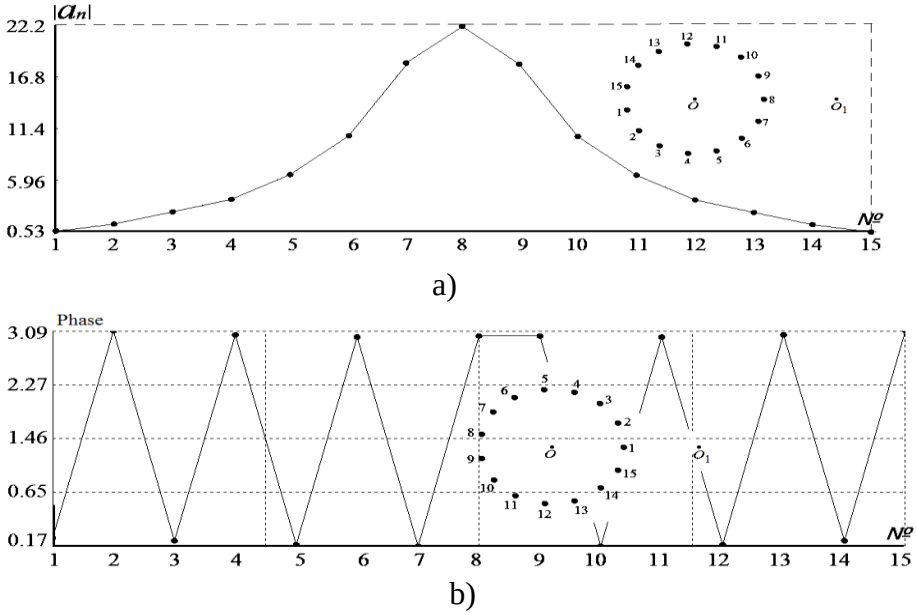

Figure 11. The character of the sources complex amplitudes: a) distribution of absolute values, b) distribution of phases.

It should be noted that each subsequent source is almost in antiphase with the previous source, which together ensures the formation of a high amplitude reactive field. In addition, the phases of sources with even (as well as odd) numbers differ from each other by a very insignificant value. It is this phase shift that ensures the transition of a small part of the reactive field energy into the energy of a traveling wave with the center O_1. With a decrease in the radius of the auxiliary surface, the amplitudes of the auxiliary sources and the reactive field increase. The study showed that when the radius is halved, the amplitudes of the reactive field increase by two orders of magnitude. Hence, we can conclude that the further away the center of radiation created by the reactive field is, the higher is its amplitude.

3.2. The case of distribution of sources along a segment

Figure 12a) and 12b) show the case when 14 auxiliary sources are distributed along a horizontal segment of length $2R$, with $kR = 8$. Due to the symmetry of the field in the upper and lower half-planes, the condition of equality of the fields is required only on the upper semicircle of the radius $k\tilde{R} = 15$. Comparing with the previous case, only the form of the internal reactive field has changed, and the external field again has a radiation

center O_1. In this case, $k\rho_0 = 10$. The animation of the internal field also showed the presence of an imaginary source field in it, that is, it "seeps" through the reactive field. If we subtract from the obtained field the field of a point source centered at O_1, then the remaining part has a "breathing", non-propagating character, i.e., it is only a standing reactive field [20].

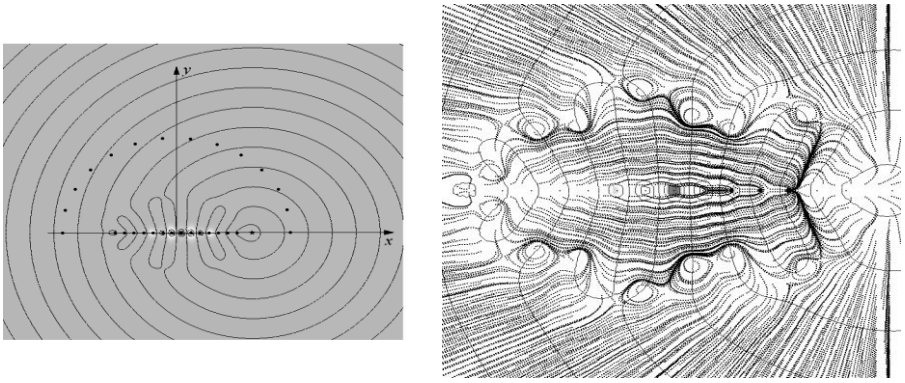

a) b)

Figure 12. Obtaining the imaginary source by 14 sources on the line: a) the inner and outer fields, b) the Poynting vector lines in the inner area.

Analysis of the complex amplitudes of the auxiliary sources shows that they take on large values in comparison with the amplitude of the point source, the field of which they form in the far zone. As in the addition theorem, the sum of these amplitudes is equal to unit, i.e., the balance of the total current is observed. The figure13a) and 13b) show the corresponding absolute values of the amplitudes of the sources and their phases. It can be seen that the sources located in the middle of the segment have the maximum amplitude.

In this case, neighboring sources are also almost in antiphase. You can notice the presence of a phase shift between even numbered sources (as well as odd ones). This phase shift is of little value, however, as in the previous case, it is this shift that ensures the transfer of a small part of the internal energy to the external region in the form of a field of a point source.

3.3. Obtaining two imaginary centers of field radiation

The following is the case when 15 auxiliary sources on a circle of radius $kR = 2$, describe the external field of two sources at points $O'(x', y')$ and $O''(x'', y'')$ (Figure 14). In this case $kx' = kx'' = 4$, $ky' = -ky'' = -2$. The figure 15 shows the same external field described by 20 auxiliary sources on a curve of a more complex shape (Cassini oval).

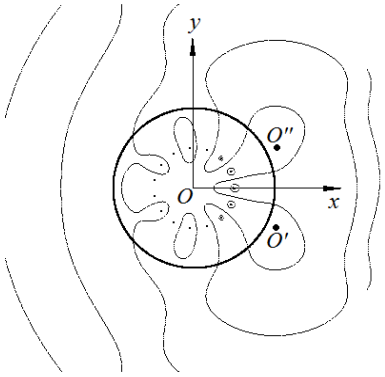

Figure 14. Obtaining two imaginary sources field by sources on the circle.

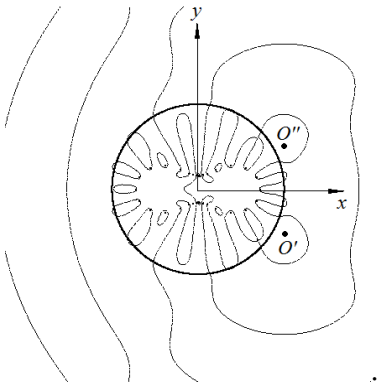

Figure 15. Obtaining two imaginary sources field by sources on the Cassini oval.

From these results, it can be concluded that the described method can be used to obtain the field not only of a point source, but also of two or more sources, i.e., fields of a more complex type.

For simplicity of visualization and calculations, two-dimensional cases have been considered so far. However, the ideas of the work remain valid in the three-dimensional case, considered below.

3.4. Three-dimensional case

225 Hertz dipoles are uniformly distributed on a sphere of radius $kR = 2$. The values of their complex amplitudes are found, which ensure the formation of a Hertz dipole field of unit amplitude, with a polarization vector along the *OZ* axis and with a pole at the point $O_1(r_0, 0, 0)$ where $kr_0 = 4$. The radius of the sphere, on which the condition of equality of fields is required, is defined as $k\tilde{R} = 10$. The figure16 shows the

distribution of the E_z component of the field, with a clearly visible region of the reactive part.

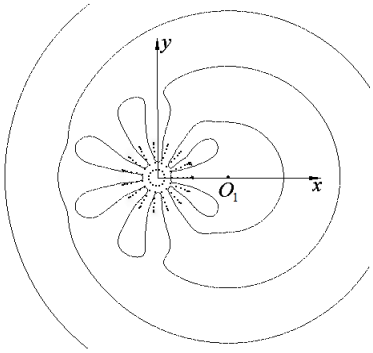

Figure 16. Obtaining the imaginary source field by auxiliary sources on the sphere.

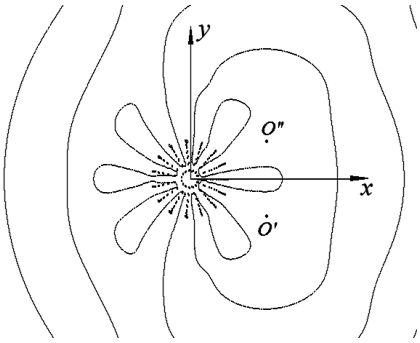

Figure 17. Obtaining two imaginary sources field by auxiliary sources on the sphere.

Next, we consider the same case of a spherical auxiliary surface, with the same radius and with the same number of auxiliary sources. In this case, such values of their complex amplitudes have been found that ensure the formation of the field of two Hertz dipoles located at points $O'(x', y', 0)$ and $O''(x'', y'', 0)$, polarized along the *OZ* axis. The coordinates of these points are defined as $kx' = kx'' = 4$, $ky' = -ky'' = -2$. The figure 17 shows the distribution of the E_z component of the field.

6. CONCLUSION

In this paper it is shown that the location of the singularities of the analytical wave field and its real sources do not always coincide. This shift is due to the presence of reactive fields of real sources that form a singularity in another region. It is shown that such reactive fields have a high energy and amplitude compared to the field of a traveling wave, but due to their rapid decrease, they do not participate in the far zone. By constructing an analytical continuation of the far field, it is shown that an external observer can see only the singularity created by the reactive field, but not the field itself or its sources. The presence of vortices of the Poynting vectors force lines of the reactive field is explained by the existence of areas with counter energy flows. Two-dimensional and three-dimensional cases are considered.

ACKNOWLEDGEMENTS

This work was carried out with the financial support of the Georgian National Fund named after Sh. Rustaveli (Grant YS-19-570).

REFERENCES

[1] J. A. Stratton, "Electromagnetic Theory", Moscow, 1948.

[2] R. S. Zaridze, V. A. Tabatadze, I. M. Petoev-Darsavelidze, and G. V. Popov, "Determination of the Location of Field Singularities Using the Method of Auxiliary Sources", Journal of Communications Technology and Electronics, 2019, Vol. 64, No. 11, pp. 1170–1178.

[3] Petoev-Darsavelidze, V. Tabatadze, R. Zaridze, M. Prishvin, "Investigation of the Reactive Field's Some Properties", XXIVth International Seminar/Workshop on Direct and Inverse Problems of Electromagnetic and Acoustic Wave Theory (DIPED-2019), Lviv, Ukraine, September 12-14, 2019, pp. 13-19

[4] N. Vadachkoria, V. Tabatadze, R. Zaridze, I. Petoev "Active Sources Localization by Measured Field", DIPED 2016, Tbilisi, Georgia, September 26-29, 2016, pp. 133 – 137.

[5] V. Tabatadze, R. Zaridze, B. Poniava, T. Tchabukiani, "Application of the MAS in the 3D Antenna Synthesis Problems", DIPED-2015, Lvov, 2015, pp. 85-89.

[6] R. Zaridze, V. Tabatadze, I. Petoev, T. Tchabukiani, "Optimal Antenna Synthesis Problem Solution Using the Method of Auxiliary Sources", International Conference on Microwaves, Communications, Antennas and Electronic Systems.

[7] R. S. Zaridze, I.M. Petoev, V.A. Tabatadze, B.V. Poniava, "The Method of Auxiliary Sources for antenna synthesis problems". Proceedings of XVIII-th International Seminar/Workshop on Direct and Inverse Problems of Electromagnetic and Acoustic Wave Theory (DIPED-2013), September 23-26, 2013, Lviv, Ukraine. pp. 13-19.

[8] D. Ding, J. Xia, L. Yang, X. Ding, "Multiobjective Optimization Design for Electrically Large Coverage", IEEE AP Magazine, Vol. 60, No. 1, 2018. pp. 27-37.

[9] A. Michel, P. Nepa, X. Qing, Z. Ning Chen, "Considering High-Performance Near-Field Radar Antennas", IEEE AP Magazine, Vol. 60, No. 1, 2018. pp. 14-26.

[10] Sh. Arakelyan, H. Lee, A. Babajanyan, S. Kim, G. Berthiau, B. Friedman, K. Lee, "Antenna Investigation by a Thermoelastic Optical Indicator Microscope", IEEE AP Magazine, Vol. 61, No. 2, 2019. pp. 27-31.

[11] Купрадзе В.Д. // Успехи мат. наук. 1967. Т. 22. № 2. с. 59.

[12] Vekua I.N. // Rep. Acad. Sci. USSR. 1953 V. 90. № 5. p. 715.

[13] Zaridze R., Bit-Babik G., Tavzarashvili K., et al. //IEEE Trans. 2002. V.AP 50. № 1. P. 50.

[14] Tabatadze V., Bijamov Jr.A., Kakulia D., et al. // Int. J. Infrared and Millimeter Waves. 2008. V. 29. № 12. p. 1172.

[15] Rolland A., Kakulia D., Petoev I., et al. // Proc. 11th Int. Conf. on Mathematical Methods in Electromagnetic Theory (MMET 2008), Odessa 29 Jun.–02 July. 2008. N.Y.: IEEE, 2008, p. 208.

[16] Tabatadze V., Petoev I., Zaridze R. // Proc. 13th Int. Conf. on Mathematical Methods in Electromagnetic Theory (MMET 2010). Kyiv. 6–8 Sep. 2010. N.Y.: IEEE, 2010.

[17] Petoev I., Tabatadze V., Zaridze R. // Proc. 5th Eur. Conf. on Antennas and Propagation (EUCAP), 2011, Rome, Italy. p. 1157.

[18] Zaridze R., Bit-Babik G., Karkashadze D., et al. The Method of Auxiliary Sources (MAS). Solution of Propagation, Diffraction and Inverse Problems Using MAS. Athens: Institute of Communication and Computers Systems, 1998.

[19] I. S. Gradshteyn, I. M. Ryshik, "Table of Integrals, Series, and Products", Moscow, 1963.

[20] http://lae.tsu.ge/